Journal of Power Sources 220 (2012) 342–347

Contents lists available at SciVerse ScienceDirect

Journal of Power Sources

journal homepage: www.elsevier.com/locate/jpowsour

Short communication

Synthesis of cage-like $LiFePO_4$/C microspheres for high performance lithium ion batteries

Honggui Deng, Shuangling Jin, Liang Zhan*, Yanli Wang, Wenming Qiao, Licheng Ling*

State Key Laboratory of Chemical Engineering, East China University of Science and Technology, Meilong Road 130, Shanghai 200237, PR China

HIGHLIGHTS

- Cage-like $LiFePO_4$/C microspheres (cage-like LPCs) were synthesized.
- The unique structures offer cage-like LPC electrode with high rate performance.
- The microstructures of cage-like LPCs are very stable with a diameter of 1.6 μm.
- The reversible capacity of cage-like LPCs can maintain 160 mAh g^{-1} at 0.1 C.
- The reversible capacity of cage-like LPCs is as high as 120 mAh g^{-1} at 10 C.

GRAPHICAL ABSTRACT

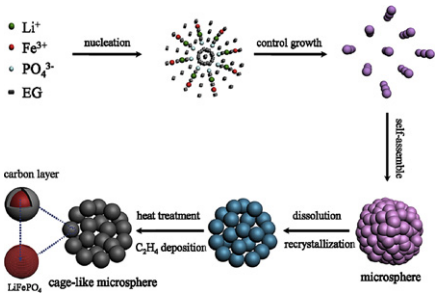

ARTICLE INFO

Article history:
Received 14 February 2012
Received in revised form
29 June 2012
Accepted 17 July 2012
Available online 11 August 2012

Keywords:
Lithium iron phosphate
Microspheres
Cathode material
Lithium ion batteries

ABSTRACT

Cage-like $LiFePO_4$ microspheres are synthesized by a solvothermal reaction–calcination process, using $Fe(NO_3)_3 \cdot 9H_2O$ as iron source and ethylene glycol/water as co-solvent medium. The microsphere is the assembly of $LiFePO_4$ nanoparticles with an open porous structure, thus the carbon coating can be easily introduced on the surface of the nanoparticles by the chemical vapor deposition of C_2H_4 during calcination process. When used as the cathode materials for the lithium-ion batteries, the resultant cage-like $LiFePO_4$/C microsphere shows high capacity and good cycle stability (160 mAh g^{-1} at 0.1 C over 300 cycles), as well as good rate capability (120 mAh g^{-1} at 10 C). The desirable electrochemical performance can be attributed to high rate of ionic/electronic conduction and the high structural stability arising from the interconnected open pores, carbon-coated nanoparticles and microsized structure.

1. Introduction

Lithium ion batteries, as power sources for portable electronic devices and electric/hybrid vehicles, have attracted tremendous attention in the scientific and industrial fields due to their high electromotive force and high energy density. To meet the increasing demand of batteries with higher energy density, higher power density and longer cycle life, many efforts have been made to develop new electrode materials or design novel structures for electrode materials [1–3]. Recently, olivine-type $LiFePO_4$ has been widely researched as a cathode material for lithium storage owing to its high theoretical capacity (170 mAh g^{-1}), thermal stability, nontoxicity, safety and low cost [4–7]. However, the inherent electronic conductivity ($\sim 10^{-9}$ S cm^{-1}) and Li-ion diffusion coefficient ($\sim 1.8 \times 10^{-14}$ cm^2 s^{-1}) of $LiFePO_4$ are much low at room temperature, which largely prevent its high-rate performance [8,9].

Modifications of $LiFePO_4$ particles by minimizing the particle size and coating them with an electron-conducting carbon layer are

* Corresponding authors. Tel.: +86 21 64252924; fax: +86 21 64252914.
E-mail addresses: zhanliang@ecust.edu.cn (L. Zhan), lcling@ecust.edu.cn (L. Ling).

0378-7753/$ – see front matter
http://dx.doi.org/10.1016/j.jpowsour.2012.07.060

considered to be effective in surmounting electronic and ionic transport limitations [10,11]. By combining both of these approaches, many synthesis methods, including mechanochemical activation [10,12], sol–gel [13,14], hydrothermal/solvothermal [15–20], etc., have been developed to prepare nanosized $LiFePO_4$/C composite materials. Furthermore, smaller $LiFePO_4$ nanoparticles coated with optimized amount of carbon in a porous or loose structure is advantageous to achieving unhindered contact of electrolyte resulting in better electrode performance. For example, Kang et al. [11] had reported an inorganic-based sol–gel method to synthesize carbon-coated $LiFePO_4$ nanoparticles, which exhibited a capacity of about 162.7 mAg h^{-1} and good cycling stability at 0.1 C, when the carbon content is 4.5%. However, the low tap density resulting from the nanoparticles limits the total volumetric energy density which is also quite important for practical applications. Generally, it is believed that the microsized spherical particles can easily be closely packed [21]. In this regard, a microsized porous sphere comprising of carbon-coated $LiFePO_4$ nanoparticles is proposed as an optimal structure for $LiFePO_4$ to realize high performance without compromising the packing density [22–27].

Herein, we developed an alternative approach to the synthesis of cage-like $LiFePO_4$/C microspheres (denoted as cage-like LPCs) via a solvothermal reaction combined with calcination, using inexpensive and stable $Fe(NO_3)_3 \cdot 9H_2O$ as iron source and ethylene glycol/water as co-solvent medium. The resultant cage-like LPCs are consisted of carbon coated nanoparticles with an interconnected open porous microstructure. Such unique features can provide more channels for the rapid diffusions of Li ion and prevent the aggregation of $LiFePO_4$ particles during charging and discharging processes. Therefore, this $LiFePO_4$/C composite not only show excellent high-rate performance, but also have a relatively high tap density.

2. Experimental

2.1. Materials preparation

All chemicals were purchased from Sinopharm Chemical Reagent Co., Ltd. and used without further purification. In a typical synthesis, 0.015 mol of Li_2SO_4, 0.01 mol of $Fe(NO_3)_3 \cdot 9H_2O$ and 0.005 mol of P_2O_5 were added in a Teflon vessel together with 40 mL ethylene glycol (EG) and 20 mL deionized water. After vigorous stirring for 0.5 h, the vessel was sealed in a stainless-steel autoclave, then placed inside an oven and heated at 180 °C for 24 h. Afterward, the precipitates were collected by centrifugation and dried at 80 °C for 72 h in vacuum atmosphere. The obtained product was calcined at 600 °C under flowing Ar/H_2 atmosphere (100 mL min^{-1}, 95 vol. % Ar and 5 vol. % H_2) for 10 h, and for the carbon coating, the gas was then switched to C_2H_4/Ar (20 mL min^{-1}, 50 vol. % C_2H_4 and 50 vol. % Ar) for 15 min. To investigate the formation process of the cage-like LPCs, time-dependent experiments were carefully conducted. And the experimental parameters, such as the phosphate sources and the solvent, were also varied during the synthesis to study their effects on the shape of the final product. Commercial $LiFePO_4$/C sample (particle size around 2–3 μm, carbon content about 5.2%) was purchased from Tianjin Sterlan-Energy Ltd., China.

2.2. Materials characterization

Powder X-ray diffraction (XRD) patterns were recorded using a Bruker AXS D8 diffractometer using Cu Kα radiation with 2θ in a range of 10–70° in steps of 0.05°. Raman spectra were obtained from a Renishaw inVia + Reflex Raman spectrometer with 514 nm laser radiation at a laser power of 0.48 mW in the range of 400–2000 cm^{-1}. Measurement of carbon content was carried out on a Thermogravimetric analyzer (TGA), and data were recorded from ambient to 650 °C at a heating rate of 5 °C min^{-1} in air. The microstructures of samples were observed using a FEI Quanta 200 scanning electron microscope (SEM) and a JEOL TEM-2000FXII transmission electron microscope (TEM). Before measurement, TEM samples were ultrasonically treated in a solution of ethanol. The pore structures were carried out using an ASAP 2020 Micromeritics surface area analyzer. To measure the tap density, a certain amount of the sample was placed in a small measuring cylinder and tapped for at least 10 min by hand. The measured volume of the tapped powder and its mass were used to calculate the tap density.

2.3. Electrochemical measurements

A composite electrode used for electrochemical measurements was prepared by mixing the active material, carbon black and poly (vinylidene fluoride) (PVDF) in weight ratio of 75:15:10 using N-methyl-2-pyrrolidone (NMP) as solvent. Lithium foil was used as the counter and reference electrode. The obtained slurry was then cast onto aluminum foil with the electrode thickness of 20 μm. The electrode area was 1.1 cm^2 and the mass loading of the $LiFePO_4$ was about 3.5 mg cm^{-2}. The electrolyte was a solution of 1 M $LiPF_6$ dissolved in ethylene carbonate (EC)/diethyl carbonate (DEC) (1:1 V/V) and the separator was Celgard 2400. The CR2016 coin-type cell was assembled in an argon-filled glove box, using Li metal as the counter electrode. Galvanostatic charge/discharge tests were conducted in the voltage range of 2.5–4.2 V versus Li/Li^+ on the CT2001A LAND Battery Tester. Cyclic voltammograms (CVs) were recorded between 2.5 and 4.1 V at a scan rate of 0.1 mV s^{-1} on an Arbin BT2000 electrochemical workstation. The capacity of the material was calculated with the mass of $LiFePO_4$, not including the carbon content.

3. Results and discussion

To elucidate the morphology and structure of the product, SEM and TEM measurements were carried out. As shown in Fig. 1a and b, the uniform and monodisperse microspheres can be clearly observed with the diameter of about 1.6 μm. More interestingly, the resultant microspheres are constructed by numerous nanoparticles with the size of about 100 nm. And there are abundant interstitial spaces between nanoparticles with the pore size of about 200 nm, giving cage-like architectures. It should be noted that the microstructures of cage-like LPCs are so stable that they cannot be destroyed into fragments or dispersed into nanoparticles even after the ultrasonic treatment. The distinct contrast between the central and fringe part of an individual architecture implies that there are abundant pores distributed throughout in the microspheres (Fig. 1c). High resolution TEM (HRTEM) images of the surface in the exterior (Fig. 1d) and the outer edges of the framework (Fig. 1e) further affirm that the surfaces of the $LiFePO_4$ are covered by a layer of amorphous carbon with a thickness of 2 nm. In addition, the d-spacing values of the adjacent lattice as shown in Fig. 1e are 0.52 nm, agreeing well with the (020) plane of orthorhombic phase of $LiFePO_4$ [5]. The selected area electron diffraction (SAED, Fig. 1f) further reveals that the single $LiFePO_4$ particle is well crystallized with pure olivine phase.

To further investigate the porous structure of the cage-like LPCs, the adsorption/desorption isotherms measurements are conducted. As shown in Fig. 2a, a distinct hysteresis loop in the P/P_0 range of 0.4–0.9 suggests the existence of mesopores. The Brunauer–Emmett–Teller (BET) surface area calculated from the adsorption isotherm in the P/P_0 range between 0.05 and 0.30 is 35.5 m^2 g^{-1}. And the corresponding BJH pore-size distribution

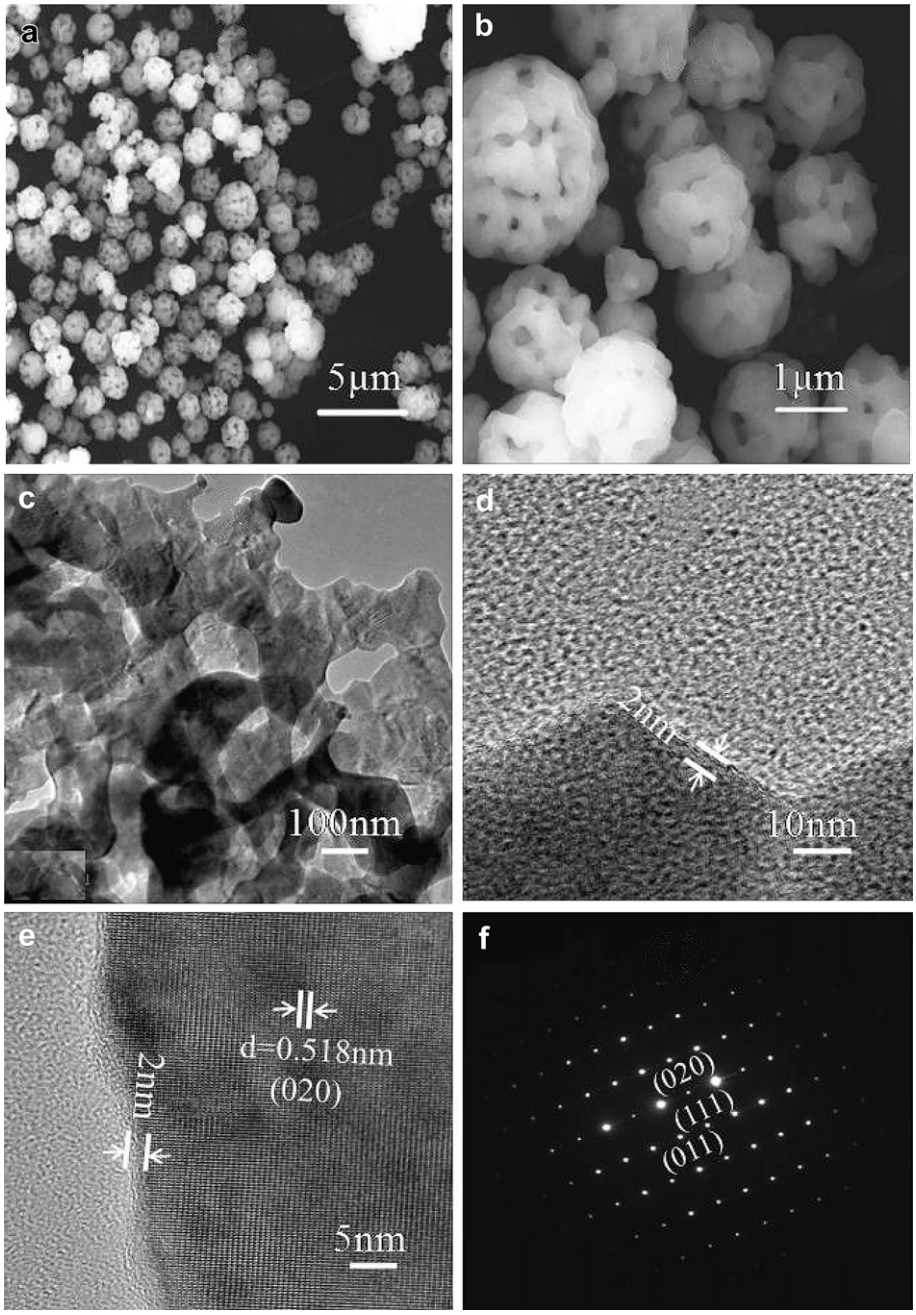

Fig. 1. SEM (a, b), TEM (c) and HRTEM (d, e) and SAED (f) images of the cage-like LPCs.

(inset in Fig. 2a) demonstrates the presence of the complex hierarchical pores including mesopores and macropores.

The XRD pattern and the Rietveld refinement of the cage-like LPCs sample are shown in Fig. 2b. There is a good correspondence to the orthorhombic olivine phase (space group: *Pnma*) with well crystallized characteristics. The good fit between the observed and calculated patterns demonstrates that a single phase is obtained with no evidence of impurities, such as Fe_2O_3 and $Li_3Fe_2(PO_4)_3$, although Fe^{3+} source was used. No significant signal is associated with carbon, possibly because the carbon layer around $LiFePO_4$ particles is amorphous and thin.

Raman spectroscopy was further performed to analyze the phase composition of the cage-like LPCs sample, as shown in Fig. 2c. Two intense broad peaks located at 1325 and 1598 cm^{-1} are respectively attributed to the A_{1g} vibration mode of the disordered carbon (D-band) and the E_{2g} vibration mode of the ordered graphitic carbon (G-band), suggesting carbon was successfully deposited on the surface of the $LiFePO_4$ particles. There is also one small peak at 950 cm^{-1}, which is assigned to the intramolecular stretching mode of PO_4^{3-}. Thermogravimetric (TG) measurement was used to estimate the carbon content in the cage-like LPCs. Fig. 2d gives the TG curve of the cage-like LPCs sample in air. It should be mentioned that, in the temperature range of 250–500 °C, the olivine $LiFePO_4$ can be oxidized to $Li_3Fe_2(PO_4)_3$ and Fe_2O_3, corresponding to a theoretical weight gain of 5.07%, based on the following Eq. (1) [28]:

$$LiFePO_4 + 1/4O_2 = 1/3Li_3Fe_2(PO_4)_3 + 1/6\ Fe_2O_3 \quad (1)$$

While for the $LiFePO_4$/C composite, the equation will be

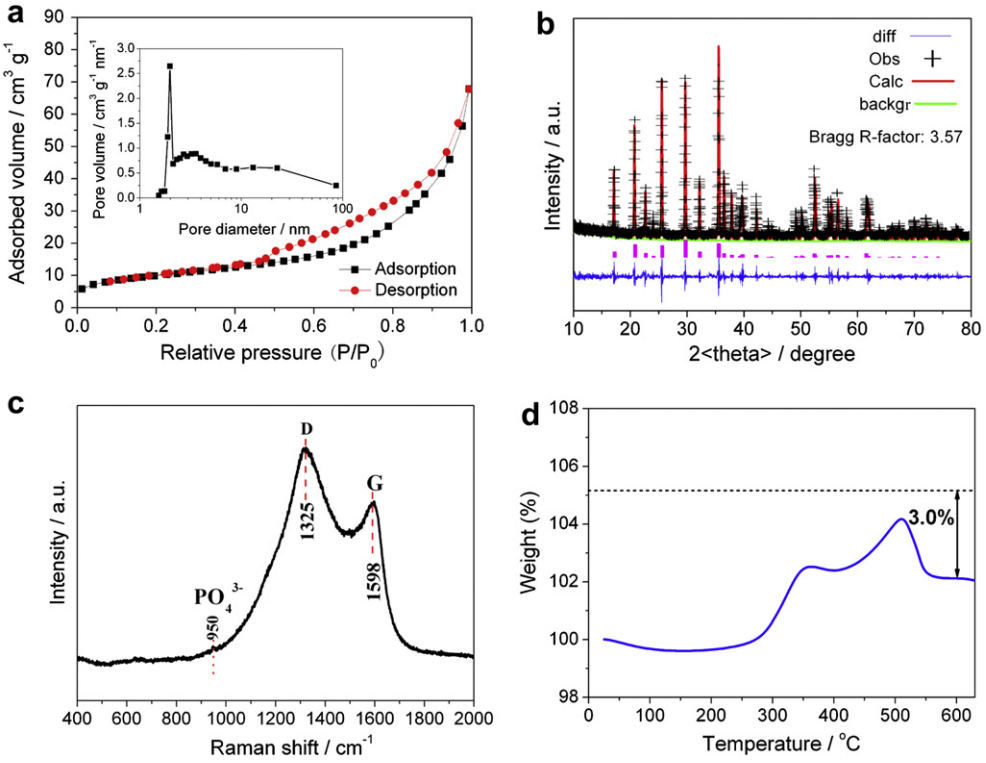

Fig. 2. Pore structure characteristics (a), XRD pattern and Rietveld refinement (b), Raman spectra (c) and TG curve (d) of the cage-like LPC sample.

$$LiFePO_4 + 1/4O_2 + xC + xO_2 = 1/3\ Li_3Fe_2(PO_4)_3 + 1/6Fe_2O_3 + xCO_2 \quad (2)$$

where x denotes the carbon content in the composite. As for the cage-like LPCs, when the sample is heated above 350 °C, the carbon in the mixture is oxidized to CO_2 gas, leading to a weight loss. Above 500 °C, a total oxidization of both $LiFePO_4$ and carbon is completed. Finally, by considering the theoretical weight gain (5.07%) of pure $LiFePO_4$ during TG measurement in air, the amount of carbon in the cage-like LPCs sample is calculated to be about 3.0%. Combined with the results of HRTEM in Fig. 1d and e, it can be concluded that a thin layer of amorphous carbon was coated on the surface of $LiFePO_4$ particles.

In order to understand the formation process of $LiFePO_4$ hierarchical microstructures, time-dependent experiments were carried out to clarify the formation mechanism. Support Information Fig. S1 displays SEM observations of the solvothermal reaction products at different reaction time periods. At the initial stage (15 min), the product is composed of nanoparticles with the average size of about 50 nm (Fig. S1a). As the reaction proceeds to 1.5 h (Fig. S1b), no nanoparticles remain and the monodisperse microspheres consisted of many tight packed nanoparticles become the exclusive products. When the reaction time is further prolonged to 5 h, as shown in Fig. S1c, the surfaces of the resulting microspheres become rough, indicating the microsphere may undergo a dissolution–recrystallization process, etching the densely packed spheres into a relatively loose structure. Further increasing the reaction time to 24 h, the nanoparticles on the spheres grow larger and the incompact porous structure becomes even more evident (Fig. S1d). On the basis of the above time-dependent experimental evidence, the formation process of the $LiFePO_4$ precursor microspheres is illustrated in Fig. 3, which involves a nucleation and aggregation of primary particles followed by a dissolution–recrystallization process. At the beginning of the reaction, the precursor nuclei quickly grow into the primary particles and these freshly nanoparticles aggregate together to form the densely packed microspheres driven by the minimization of interfacial energy of system. With prolonged solvothermal treatment, the agglomerated $LiFePO_4$ precursor undergoes a dissolution–recrystallization process, in which the dissolution–diffusion process offers the opportunity to create the porosity on the densely packed microspheres. Moreover, some control experiments were carried out by replacing some amount of EG with ethanol, glycerol and water as the solvent or using $(NH_4)_3PO_4$ and $NH_4H_2PO_4$ instead of P_2O_5 as phosphate source with other conditions constant. The SEM images of the resulting products are shown in Support Information Fig. S2 and S3, which demonstrate that both EG and P_2O_5 are essential for the formation of such hierarchical $LiFePO_4$ microstructures.

As cathode material for lithium ion batteries, the electrochemical performances of the cage-like LPCs were investigated. In the CV curves (Fig. 4a), the cage-like LPCs electrode has only one pair of peaks, corresponding to the charge/discharge reaction of the Fe^{3+}/Fe^{2+} redox couple. During the first cycle, the reduction and oxidation peaks appear at 3.32 and 3.59 V, respectively, resulting in a small potential separation of 0.27 V. This result suggests that the cage-like LPCs electrode has low polarization and good electronic conductivity, which is mainly attributed to cage-like porous structure and the nanosized primary particle with the carbon coating. Interestingly, it can be observed that the intensity of the reduction peak increased during the third scan, indicating a possible activating process in the electrode material [29,30].

Fig. 4b shows the cycle performance of the cage-like LPCs electrode at a rate of 0.1 C. The electrode delivers a discharge capacity of 161 mAh g^{-1} in the first cycle, and still maintains 160 mAh g^{-1} after 300 cycles, suggesting that the cage-like LPCs electrode has high reversible capacity, structural stability and

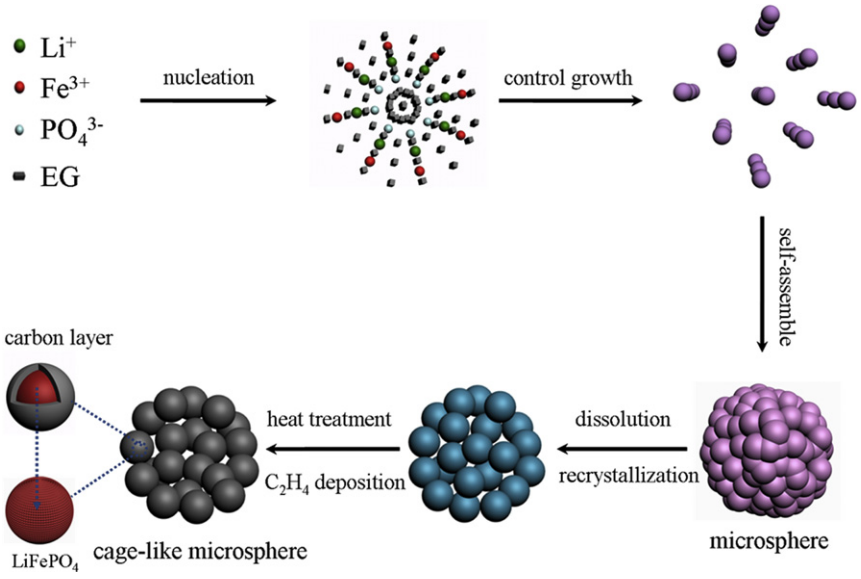

Fig. 3. Schematic illustration of the cage-like LPCs.

excellent cycling stability. Additionally, the charge/discharge profiles of different cycles at 0.1 C are shown in the inset. The long and flat voltage plateaus at 3.46 and 3.40 V are observed during charge and discharge processes, respectively, corresponding to the two-phase redox reaction between $FePO_4$ and $LiFePO_4$. The voltage difference (60 mV) between the charge and discharge plateaus has no increase with the cycle number increasing, indicating the electrode has a low polarization.

The rate performance of the cage-like LPCs electrode is further investigated over the range from 0.1 to 10 C. For comparison, the commercial $LiFePO_4$/C sample is also tested under the same conditions. The SEM images, as shown in Fig. S4a and b (Support Information), reveal that the commercial sample is composed of micrometer-sized irregular particles with the average agglomerate size of 2–3 μm. And the TG measurement demonstrates the carbon content in the commercial sample is about 5.2%. Fig. 4c and d exhibit the discharge capacity and cycling performances of the two samples at different C-rates. It can be seen that the cage-like LPCs electrode shows a higher specific capacity under all different current rates. Besides, although both of the samples have good cycling stability at different current rates, they exhibit quite different capacity decay with the enhanced rate. As for the cage-like LPCs electrode, the reversible

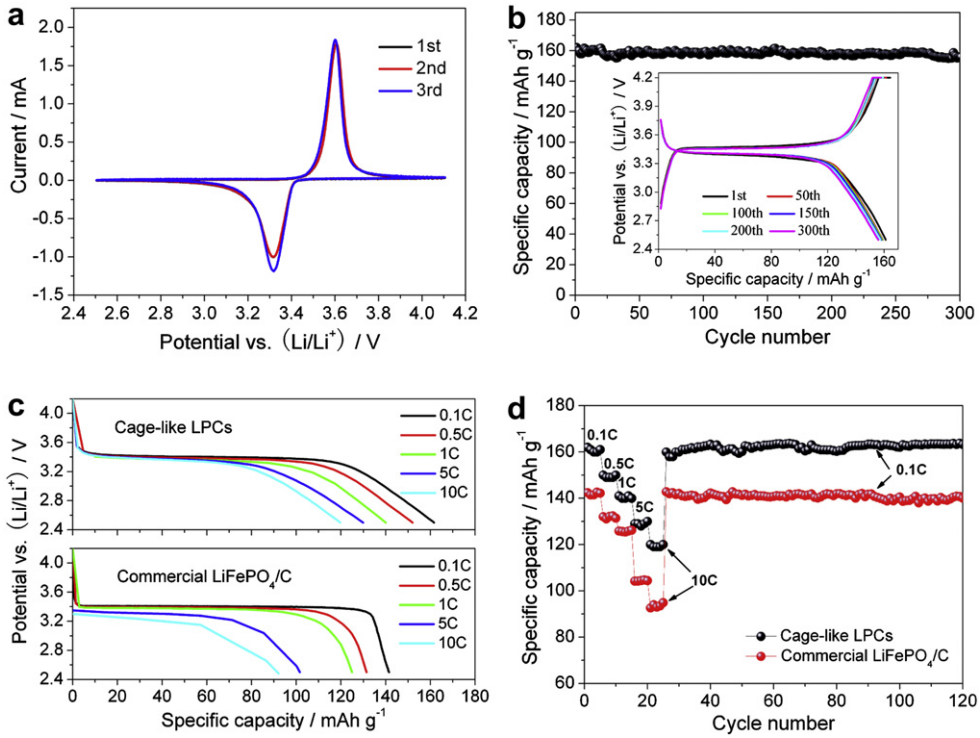

Fig. 4. (a) Cyclic voltammograms of the cage-like LPC electrode at a scan rate of 0.1 mV s^{-1}. (b) Cycle performance of the cage-like LPC sample in the voltage range from 2.5 to 4.2 V at the current rate of 0.1 C. Inset: Charge/discharge profiles of different cycles at 0.1 C. (c) Discharge/charge profiles of the cage-like LPC and commercial $LiFePO_4$/C electrodes at different current rates. (d) The rate and cycling performances of the cage-like LPC and commercial $LiFePO_4$/C electrodes.

capacities at 0.5, 1, 5 and 10 C rate are about 150, 140, 130 and 120 mAh g^{-1}, which are 93, 87, 80 and 75% of the initial discharge capacity at 0.1 C, respectively. And when the current rate is again reduced back to 0.1 C, the reversible capacity can be recovered and maintains at 160 mAh g^{-1}. Compared with the cage-like LPCs sample, when the current rate is increased to 5 and 10 C rates, the commercial $LiFePO_4$/C electrode only presents 72 and 65% of the discharge capacity at 0.1 C, respectively. From the above analysis, the excellent electrochemical performance of the cage-like LPCs can be ascribed to their unique nano/micro hierarchical microstructures. The open porous structure guarantees the quick penetration of electrolyte to the surface of the active material and the carbon-coated nanosized primary particle affords short diffusion lengths for both Li ion and electron transport. Thus, the kinetic performance of the electrode is better, the intercalation and extraction processes are much higher efficiency, and therefore a higher effective specific capacity can be achieved. In addition, the as-obtained cage-like LPCs with a microspherical structure can easily be densely packed to give a tap density of 1.3 g cm^{-3}, which is higher than the normal $LiFePO_4$/C nanoparticles (less than 1.0 g cm^{-3}), thus can offer high rate performance without sacrificing the volumetric energy density of the electrode in the practical application.

4. Conclusions

In summary, we have successfully prepared 3D porous $LiFePO_4$/C microspheres with cage-like structure by a two-step process using inexpensive Fe^{3+} as iron source. Compared with the common synthesis for $LiFePO_4$/C composite, the carbon is introduced by chemical vapor deposition of C_2H_4 instead of secondly mixing the formed $LiFePO_4$ with other carbon source, which is much more effective and time-saving. Electrochemical measurements demonstrate that the as-obtained cage-like LPCs electrode exhibits excellent cycle stability and good rate capability, suggesting a competitive candidate for the cathode material of lithium-ion batteries. The desirable electrochemical performance should be attributed to the unique carbon coated 3D cage-like structure, which facilitates fast electrochemical reaction kinetics and good structural stability. Moreover, the microsized sphere structure of the cage-like carbon-coated $LiFePO_4$ has a high taping density for enhancing the volumetric energy density. Our ongoing work shows that this synthesis route can be extended to other useful phosphate cathode materials such as $LiMnPO_4$ and the solid solutions of $LiFePO_4$ and $LiMnPO_4$ (i.e., $LiMn_xFe_{1-x}PO_4$, $0 \leq x \leq 1$).

Acknowledgments

We thank the National Natural Science Foundation of China (51002051, 20806024, 50730003, 50672025) and, the Natural Science Foundation of Shanghai City (12ZR1407200), Fundamental Research Funds for the Central Universities (WA1014016) for financial support.

Appendix A. Supplementary material

Supplementary data associated with this article can be found, in the online version, at http://dx.doi.org/10.1016/j.jpowsour.2012.07.060.

References

[1] B. Kang, G. Ceder, Nature 458 (2009) 190–193.
[2] A.R. Armstrong, L. Christopher, P.M. Panchmatia, M.S. Islam, P.G. Bruce, Nat. Mater. 10 (2011) 223–229.
[3] A. Magasinski, P. Dixon, B. Hertzberg, A. Kvit, J. Ayala, Nat. Mater. 9 (2010) 461.
[4] J.M. Tarascon, M. Armand, Nature 414 (2001) 359–367.
[5] M. Armand, J.M. Tarascon, Nature 451 (2008) 652–657.
[6] P. Gibot, M.C. Cabanas, L. Laffont, S. Levasseur, P. Carlach, S. Hamelet, J.M. Tarascon, C. Masquelier, Nat. Mater. 7 (2008) 741–747.
[7] P.G. Bruce, B. Scrosati, J.M. Tarascon, Angew. Chem. Int. Ed. 47 (2008) 2930–2946.
[8] A. Padhi, K. Nanjundaswamy, J.B. Goodenough, J. Electrochem. Soc. 144 (1997) 1188–1194.
[9] A. Padhi, K. Nanjundaswamy, S. Okada, J.B. Goodenough, J. Electrochem. Soc. 144 (1997) 1609–1613.
[10] H.C. Shin, W.I. Cho, H. Jang, J. Power Sources 159 (2006) 1383–1388.
[11] F.Y. Kang, J. Ma, B.H. Li, New Carbon Mater. 26 (2011) 161–170.
[12] D. Zhang, R. Cai, Y.K. Zhou, Z.P. Shao, X.Z. Liao, Z.F. Ma, Electrochim. Acta 55 (2010) 2653–2661.
[13] R. Dominko, M. Gaberscek, M. Remsker, M. Remskar, D. Hanzel, S. Pejovnik, J. Jamnik, J. Electrochem. Soc. 152 (2005) A607–A610.
[14] D. Choi, P.N. Kumta, J. Power Sources 163 (2007) 1064–1069.
[15] G. Meligrana, C. Gerbaldi, A. Tuel, S. Bodoardo, N. Penazzi, J. Power Sources 160 (2006) 516–522.
[16] B. Pei, Q. Wang, W.X. Zhang, Z.H. Yang, M. Chen, Electrochim. Acta 56 (2011) 5667–5672.
[17] C.Y. Nan, J. Lu, C. Chen, Q. Peng, Y.D. Li, J. Mater. Chem. 21 (2011) 9994–9996.
[18] K. Saravanan, M.V. Reddy, P. Balaya, H. Gong, B.V.R. Chowdari, J.J. Vittal, J. Mater. Chem. 19 (2009) 605–610.
[19] K. Saravanan, P. Balaya, M.V. Reddy, H. Gong, B.V.R. Chowdari, J.J. Vittal, Energy Environ. Sci. 3 (2010) 457–464.
[20] S.L. Yang, X.F. Zhou, J.G. Zhang, Z.P. Liu, J. Mater. Chem. 20 (2010) 8086–8091.
[21] H.M. Xie, R.S. Wang, J.R. Ying, L.Y. Zhang, A.F. Jalbout, H.Y. Yu, G.L. Yang, X.M. Pan, Z.M. Su, Adv. Mater. 18 (2006) 2609–2613.
[22] F. Yu, J.J. Zhang, Y.F. Yang, G.Z. Song, J. Mater. Chem. 19 (2009) 9121–9125.
[23] L.Q. Sun, M.J. Li, R.H. Cui, H.M. Xie, R.S. Wang, J. Phys. Chem. C 114 (2010) 3297–3303.
[24] S.W. Oh, S.T. Myung, S.M. Oh, K.H. Oh, K. Amine, B. Scrosati, Y.K. Sun, Adv. Mater. 22 (2010) 4842–4845.
[25] J.F. Qian, M. Zhou, Y.L. Cao, X.P. Ai, H.X. Yang, J. Phys. Chem. C 114 (2010) 3477–3482.
[26] J. Liu, T.E. Conry, X.Y. Song, M.M. Doeff, T.J. Richardson, Energy Environ. Sci. 4 (2011) 885–888.
[27] C.W. Sun, S. Rajasekhara, J.B. Goodenough, F. Zhou, J. Am. Chem. Soc. 133 (2011) 2132–2135.
[28] I. Belharouak, C. Johnson, K. Aimne, Electrochem. Commun. 7 (2005) 983–998.
[29] Y.Q. Wang, J.L. Wang, J. Yang, Y.N. Nuli, Adv. Funct. Mater. 16 (2006) 2135–2140.
[30] X.F. Guo, H. Zhan, Y.H. Zhou, Solid State Ionics 180 (2009) 386–391.